Imaging and Harnessing Percolation at the Metal–Insulator Transition of NdNiO 3 Nanogaps

Jin Hong Lee, Felix Trier, Tom Cornelissen, Daniele Preziosi, Stéphane Fusil, Karim Bouzehouane, Sergio Valencia, Manuel Bibes

Imaging and harnessing percolation at the metal-insulator transition of $NdNiO_3$ nanogaps

Jin Hong Lee[1,*], Felix Trier[1], Tom Cornelissen[1], Daniele Preziosi[2], Stéphane Fusil[1], Karim Bouzehouane[1], Sergio Valencia[3] and Manuel Bibes[1,§]

[1] *Unité Mixte de Physique, CNRS, Thales, Univ. Paris-Sud, Université Paris-Saclay, 91767 Palaiseau, France*

[2] *Institut de Physique et Chimie des Matériaux de Strasbourg, Université de Strasbourg, CNRS, 67000 Strasbourg, France*

[3] *Helmholtz-Zentrum Berlin für Materialien und Energie, Albert-Einstein-Strasse 15, D-12489 Berlin, Germany*

[*] *e-mail address: jinhong.lee@cnrs-thales.fr*

[§] *e-mail address: manuel.bibes@cnrs-thales.fr*

Keywords: metal-insulator transition, phase separation, domain percolation, nanodevice

J.H.L. and F.T. contributed equally to this work.

Competition between co-existing electronic phases in first-order phase transitions can lead to a sharp change in the resistivity as the material is subjected to small variations in the driving parameter, *e.g.*, the temperature. One example of this phenomenon is the metal-insulator transition (MIT) in perovskite rare-earth nickelates. In such systems, reducing the transport measurement area to dimensions comparable to the domain size of insulating and metallic phases around the MIT should strongly influence the shape of the resistance-temperature curve. Here, we measure the temperature dependence of the local resistance and the nanoscale domain distribution of $NdNiO_3$ areas between Au contacts gapped by 260 down to 40 nm. We find that a sharp resistance drop appears below the bulk MIT temperature at ~105 K, with an amplitude inversely scaling with the nanogap width. By using X-ray photoemission electron microscopy, we directly correlate the resistance drop with the emergence and coalescence of individual metallic domains at the nanogap. Our observation provides a direct insight into percolation at the MIT of rare-earth nickelates.

Percolative electronic transport naturally occurs in heterogeneous media but can also arise in disordered systems or as a result of electronic phase separation in strongly correlated materials[1,2]. The electronic phase separation typically occurs in systems displaying a first-order metal-insulator transition (MIT)[3], as in several classes of transition metal oxides (VO_2,[4-10] V_2O_3[11] or perovskite rare-earth nickelates[12]).

Recently, with an abundant availability of fabrication, lithography and spectroscopy techniques at length scales of nanometers, the MIT behavior of transition metal oxides have been intensively investigated[13]. In the work of Sharoni *et al.*[14], multiple resistance drops or jumps within the resistance-temperature (*R*-*T*) curve were observed in VO_2 nanodevices. The maximal resistance jump size was herein found to scale inversely with device length with so-called avalanche events following a stochastic power law dependence. Another vanadium oxide compound, V_2O_3, was studied by Wang *et al.*[15] who found a similar first-order percolation driven MIT in patterned nanodevices. In nanogaps of the phase-separated ferromagnet (La, Pr, Ca)MnO_3, G. Singh-Bhalla *et al.*[16] observed multiple step-like changes of resistance and proposed the presence of possible intrinsic tunnel barriers based on a magnetic-field effect. Kumar *et al.*[17] reported a stochastic resistance switching process between two coplanar electrodes deposited on a polycrystalline $NdNiO_3$ (NNO) pellet.

Although the previous studies have suggested that the step-like resistance changes could originate from domain distribution based on the *R*-*T* characteristic, the direct correlation between domain distribution and resistance change still remains elusive, particularly, in perovskite rare-earth nickelates. Here, we have analyzed the device-size-dependent *R*-*T* curves of NNO nanogaps and then measured their domain evolution by utilizing an X-ray photoemission electron microscope (X-PEEM), thereby correlating the microscopic domain percolation with the macroscopic resistance change.

NNO belongs to perovskite rare-earth nickelates, a family of materials displaying a phase diagram where the MIT temperature can be tuned by the size of a rare-earth cation[18]. The MIT of NNO is first order and accordingly, the material shows a phase separation between a metallic/paramagnetic phase and an insulating/antiferromagnetic phase[19,20]; the nucleation size of metallic domains inside an insulating matrix domains has been observed to be ~100-300 nm upon warming up across the MIT transition of NNO[20]. Therefore, when the size of NNO nanogaps becomes comparable to the nucleation size of NNO metallic domains, the *R*-*T* curve is expected to differ significantly from the bulk one due to the appearance of discernible resistance drops.

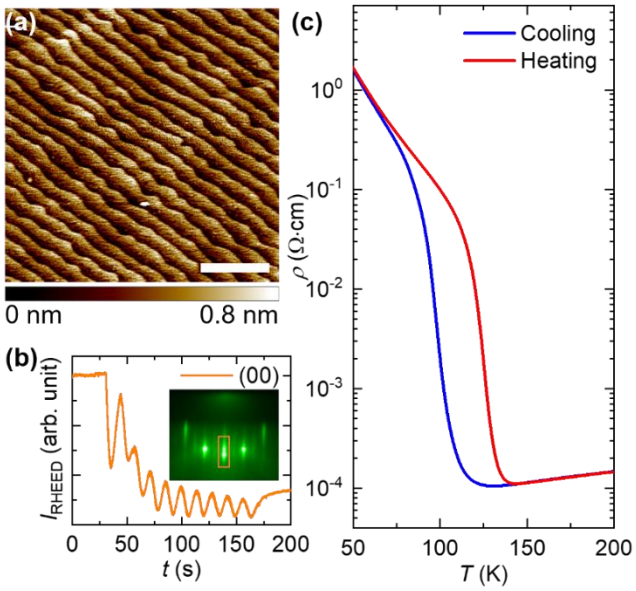

Figure 1. (a) An atomic force microscopy image of an as-grown NNO film. The scale bar represents 1 μm. (b) The RHEED intensity and pattern during the growth of film. (c) The resistivity of unpatterned NNO film as a function of temperature.

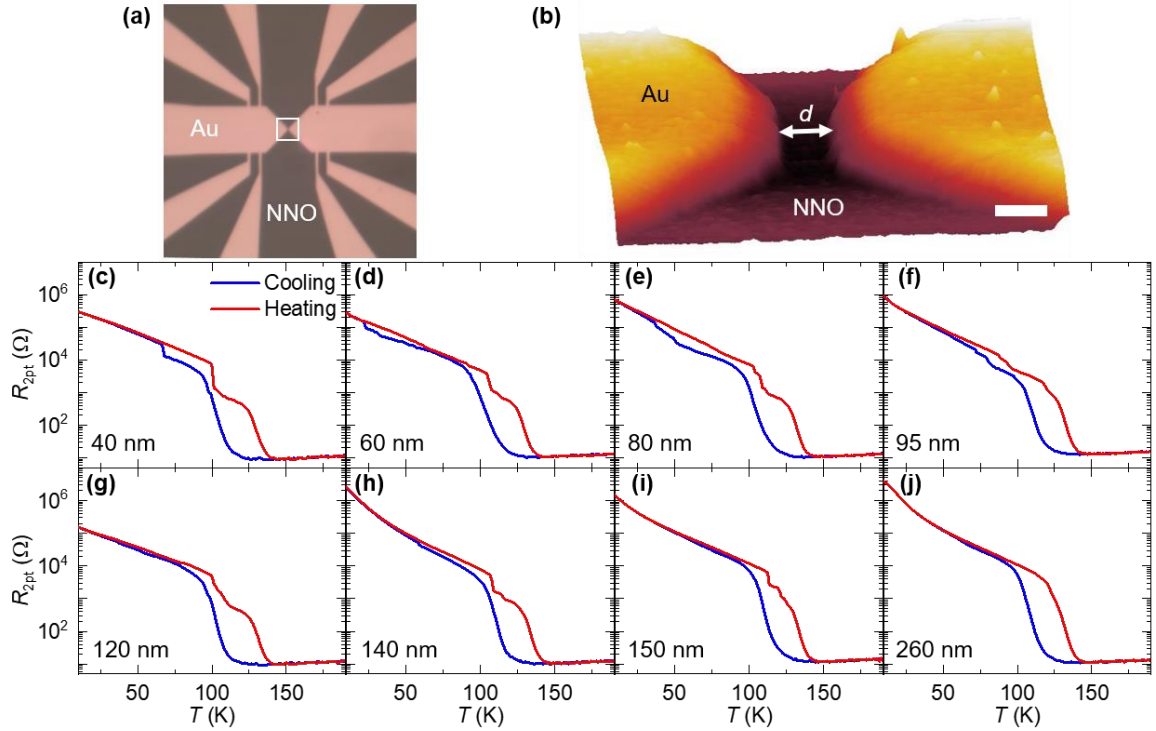

Figure 2. (a) Optical microscopy image of a NNO nanogap device. (b) AFM zoom in of the nanogap area within the white box shown in (a) where the distance between the two Au electrodes (d) is 80 nm. The scale bar represents 100 nm. (c-j) A series of R_{2pt}-T curves with d = 40 - 260 nm.

Figure 1(a) shows an atomically flat surface of the NNO film. For all devices studied, the films

are 10 unit cells thick, as determined by monitoring the intensity oscillations of the specular spot in RHEED pattern, cf (I_{RHEED}) displayed in Fig. 1(b). The streak lines in the RHEED pattern confirm the two-dimensional nature of the film surface after the growth. The bare NNO film clearly undergoes a first-order MIT characterized by four orders of magnitude change in its resistivity [Fig. 1(c)], which confirms the high quality of the film[20].

An optical microscopy image of a NNO nanogap device is shown in Fig. 2(a). Since the Au electrodes are constricted in the center of the nanogap, the measured resistance of the nanogaps mostly originates from the area between the electrodes [see the AFM image in Fig. 2(b)], where the width and length of this area is defined as d (nm) and $2d$ (nm), respectively. A series of R_{2pt}-T curves (here, R_{2pt} stands for the two-point resistance) from the nanogaps are obtained for d ranging between 40 - 260 nm, as shown in Figs. 2(c-j). All curves contain multiple R drops or jumps below the MIT temperature except the device for d = 260 nm that mimics the macroscopic behavior of NNO. In order to capture the delicate relation between d and domain evolution, we have performed two types of analysis. First, the two-exponent phenomenological percolation model[21] is applied by fitting both the insulating- and metallic-phase (I- and M-phase, respectively) regime of R_{2pt}-T heating curves with the equations from the Mott variable range hopping model and the non-Fermi liquid model, respectively, cf. below [also see the fit result in Fig. 3(a)]:

$$G_{\text{I-phase}}(T) = G_0 + G_1 \exp(-E_1 / T^{1/4}) + G_2 \exp(-E_2 / T) \tag{1}$$

$$G_{\text{M-phase}}(T) = A_1 + A_2 T \tag{2}$$

where $G_{\text{I-phase}}$ and $G_{\text{M-phase}}$ correspond to the conductance of I-phase and M-phase, and $G_{0,1,2}$, $E_{1,2}$ and $A_{1,2}$ are fitting parameters. With the two fit curves obtained, the volume fraction of I-phase, *i.e.*, $F_{\text{I-phase}}$, as a function of T [Fig. 3(b)] can be calculated by using the Bruggeman symmetric media equation[22]:

$$F_{\text{I-phase}}(T) = \frac{(G_{\text{M-phase}} - G_{\text{full}})\{G_{\text{I-phase}} + (D-1)G_{\text{full}}\}}{(G_{\text{M-phase}} - G_{\text{I-phase}})DG_{\text{full}}} \tag{3}$$

where G_{full} corresponds to the full heating curve obtained from the experiment, and D is the dimension of our system set to be 2. This two-dimensional approximation seems reasonable since the film thickness is only ~4 nm[23] and the size of M-phase domains is about two orders of magnitude higher[19,20]. In Fig. 3(c), the maximum amplitude of $F_{\text{I-phase}}$ drops, *i.e.*, $(\Delta F_{\text{I-phase}}/F_{\text{I-phase}})_{\text{max}}$ is extracted

from each R_{2pt}-T heating curve of Figs. 2(c-j), which shows that the shorter the distance between the electrodes becomes, the larger the $F_{I\text{-phase}}$ drops are observed. The second analysis exhibits the same trend by comparing the maximum R drop, *i.e.*, $(\Delta R/R)_{max}$, with electrode gap d as shown in Fig. 3(d),. Only two devices with d = 140 and 150 nm slightly deviate from this trend. This may arise from the local variation of the M-phase nucleation size in these two particular nanogaps.

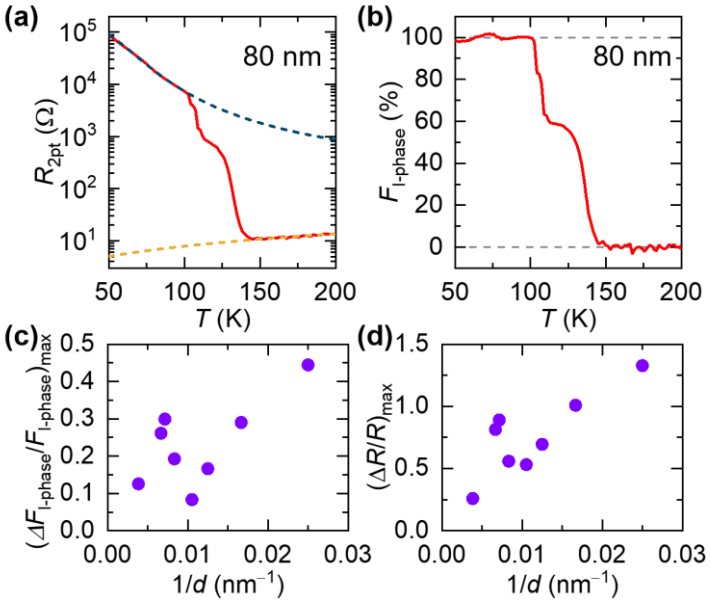

Figure 3. (a) The fit curves of I-phase and M-phase regime in the heating curve of the d = 80 nm case. (b) The extracted fraction of I-phase ($F_{I\text{-phase}}$) from the fit curves in (a). The nanogap-size-dependent (c) $F_{I\text{-phase}}$ and (d) R drops.

In order to tackle the question of whether the domain percolation inferred from the above analyses can be directly correlated with the actual domain distribution in the NNO nanogaps, we collected X-PEEM images from the nanogap of d = 80 nm at four different temperatures across the MIT. The images were obtained at two different energies of the Ni L_3 edge, where the two energies show the largest change when we plot the difference between X-ray absorption spectra (XAS) of I-phase (80 K) and M-phase (130 K): 851.6 eV (I_a) and 852.9 eV (I_b) [also see Refs. 19 and 20 for the typical shape of the low temperature XAS on NNO]. In addition, since the number of photoelectrons escaping from the nanogap was ~40% less compared with that from the outside region (probably due to a shadowing effect), the normalized intensity ratio between the two selected energies (I_a/I_b) of each pixel is obtained by removing the intensity offset between the nanogap and the surrounding region and then normalizing the I_a/I_b difference between I-phase and M-phase. The normalized full view images are displayed in Figs. 4(a-d) while Fig. 4(e) corresponds to zoomed-in view of Fig. 4(b) around the region of interest.

Since the M-phase has a relatively higher I_a compared to the case of the I-phase, the green and yellow pixels between two electrodes correspond to the domain nucleation and evolution of the M-phase. Accordingly, the blue pixels indicate the I-phase. Far below the MIT temperature [see Fig. 4(a)] the I-phase domains dominate most of the studied area, which matches well with the insulating R_{2pt}-T behavior at the same temperature in Fig. 3(a). As shown in Fig. 4(b), the nucleation and growth of the M-phase domains are observed at 100 K. More importantly, Fig. 4(e) shows that the very first metallic percolation occurs at the nanogap and this result can be related to the starting point of R drops in the R_{2pt}-T heating curve at ~105 K. Figs. 4(c) and (d) show that most of the area in the view becomes metallic after 110 K although the volume fraction of the M-phase still increases between 110 K and 120 K, which may correspond to the beginning of the bulk-like R decrease at ~125 K in the R_{2pt}-T curve.

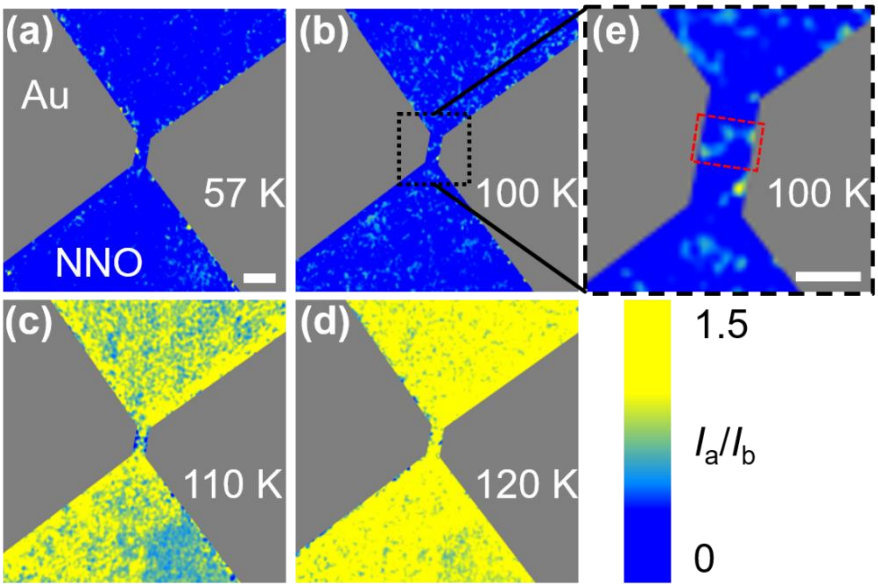

Figure 4. (a-d) The X-PEEM images showing the contrast of normalized I_a/I_b at four different temperatures, *i.e.*, 57, 100, 110 and 120 K. The scale bar in (a) represents 200 nm. (e) The zoomed-in image of the black-dashed box in (b). The red-dashed box indicates the first metallic percolation in between two Au electrodes. The scale bar represents in (e) 100 nm.

In summary, we have directly correlated the R drops appearing at the MIT of NNO nanogaps with the domain percolation behavior by combining electronic transport measurement and X-PEEM. The comparative analysis between the R_{2pt}-T curve and the X-PEEM images clearly illustrates that the observed R drops below the MIT temperature in the electronic transport measurement of NNO originates from the percolating behavior of the M-phase domains at the nanogaps. Based on our

observations, future studies such as visualizing a current-injection-driven or light-pulse-induced domain switching[24] processes in NNO nanogaps will extend our knowledge on the first-order MIT and phase separation. More generally, our finding offers a deeper understanding on the electronic transport in the nanodevices of first-order MIT materials where the domain nucleation is comparable to the size of the devices.

MATERIALS AND METHODS

10-unit-cell-thick NNO films were epitaxially grown by using pulsed laser deposition and monitored with reflection high-energy electron diffraction (RHEED) during the growth of the films. The detailed growth conditions can be found in previous references[20,25]. Following the NNO film deposition, a PMMA A6 resist soft-mask was prepared with e-beam lithography. To ensure good electrical contact between the Au electrodes and the NNO film, the NNO surface was cleaned by *in-situ* oxygen plasma exposure prior to dc magneton sputtering of 25-nm-thick Au at room temperature. Subsequently, the residual Au film was removed by lift-off leaving an area between two coplanar Au electrodes of varying size, *i.e.*, $d \times 2d$ nm^2. The *R-T* curves of the prepared NNO nanogaps were obtained by the current pulse measurement in the resistivity module of a Quantum Design Dynacool. The van der Pauw geometry was used to obtain the resistivity (ρ) of the bare NNO films before fabrication of the NNO nanogaps. The two-point resistance of the NNO nanogaps was performed with a temperature sweeping rate of 2 K/min. In order to image the local distribution of metallic (M-phase) or insulating (I-phase) domains around the NNO nanogaps, the spatially-resolved and temperature-dependent X-PEEM was performed at the UE49 PGM beamline of the BESSY II in the Helmholtz-Zentrum Berlin[26, 27].

ACKNOWLEDGMENTS

This work received support from the ERC Consolidator grant no. 615759 “MINT”, the French Research Agency (ANR) as part of the “Investissement d’Avenir” program (LABEX NanoSaclay, ref ANR-10-LABX-0035) through project “AXION”, and by the Region Ile-de-France DIM OXYMORE program through project “NEIMO”. F.T. acknowledges support by research grant VKR023371 (SPINOX) from VILLUM FONDEN. We thank HZB for the allocation of neutron/synchrotron radiation beamtime. The research leading to this result has been supported by the project

CALIPSOplus under the Grant Agreement 730872 from the EU Framework Programme for Research and Innovation HORIZON 2020.

REFERENCES

[1] Isichenko, M. B. Rev. Mod. Phys. **1992**, 64 (4), 961–1043.

[2] Stauffer, D.; Aharony, A., Introduction to Percolation Theory (Revised Second Edition). CRC Press, 1994.

[3] Imada, M.; Fujimori, A.; Tokura, Y. Rev. Mod. Phys. **1998**, 70 (4), 1039–1263.

[4] Qazilbash, M. M.; Brehm, M.; Chae, B.-G.; Ho, P.-C.; Andreev, G. O.; Kim, B.-J.; Yun, S. J.; Balatsky, A. V.; Maple, M. B.; Keilmann, F.; Kim, H.-T.; Basov, D. N. Science **2007**, 1750–1753.

[5] Qazilbash, M. M.; Brehm, M.; Andreev, G. O.; Frenzel, A.; Ho, P.-C.; Chae, B.-G.; Kim, B.-J.; Yun, S. J.; Kim, H.-T.; Balatsky, A. V.; Shpyrko, O. G.; Maple, M. B.; Keilmann, F.; Basov, D. N. Phys. Rev. B **2009**, 79, 075107.

[6] Qazilbash, M. M.; Tripathi, A.; Schafgans, A. A.; Kim, B.-J.; Kim, H.-T.; Cai, Z.; Holt, M. V.; Maser, J. M.; Keilmann, F.; Shpyrko, O. G.; Basov, D. N. Phys. Rev. B **2011**, 83, 165108.

[7] Kawatani, K.; Takami, H.; Kanki, T.; Tanaka, H. Appl. Phys. Lett. **2012**, 100, 173112.

[8] Liu, M. K.; Wagner, M.; Abreu, E.; Kittiwatanakul, S.; McLeod, A.; Fei, Z.; Goldflam, M.; Dai, S.; Fogler, M. M.; Lu, J.; Wolf, S. A.; Averitt, R. D.; Basov, D. N. Phys. Rev. Lett. **2013**, 111, 096602.

[9] Stinson, H. T.; Sternbach, A.; Najera, O.; Jing, R.; Mcleod, A. S.; Slusar, T. V.; Mueller, A.; Anderegg, L.; Kim, H. T.; Rozenberg, M.; Basov, D. N. Nat. Commun. **2018**, 9, 3604.

[10] Lee, D.; Chung, B.; Shi, Y.; Kim, G.-Y.; Campbell, N.; Xue, F.; Song, K.; Choi, S.-Y.; Podkaminer, J. P.; Kim, T. H.; Ryan, P. J.; Kim, J.-W.; Paudel, T. R.; Kang, J.-H.; Spinuzzi, J. W.; Tenne, D. A.; Tsymbal, E. Y.; Rzchowski, M. S.; Chen, L. Q.; Lee, J.; Eom, C. B. Science **2018**, 362, 1037–1040.

[11] McLeod, A. S.; Heumen, E. V.; Ramirez, J. G.; Wang, S.; Saerbeck, T.; Guenon, S.; Goldflam, M.; Anderegg, L.; Kelly, P.; Mueller, A.; Liu, M. K.; Schuller, I. K.; Basov, D. N. Nat. Phys. **2017**, 13, 80–86.

[12] Post, K. W.; McLeod, A. S.; Hepting, M.; Bluschke, M.; Wang, Y.; Cristiani, G; Logvenov, G.; Charnukha, A.; Ni, G. X.; Radhakrishnan, P.; Minola, M.; Pasupathy, A.; Boris, A. V.; Benckiser,

E.; Dahmen, K. A.; Carlson, E. W.; Keimer, B.; Basov, D. N. Nat. Phys. **2018**, 14, 1056–1062.

[13] Wei, J; Natelson, D. Nanoscale **2011**, 3, 3509–3521.

[14] Sharoni, A.; Ramirez, J. G.; Schuller, I. K. Phys. Rev. Lett. **2008**, 101, 026404.

[15] Wang, S.; Ramirez, J. G.; Schuller, I. K. Phys. Rev. B **2015**, 92, 085150.

[16] Singh-Bhalla, G.; Selcuk, S.; Dhakal, T.; Biswas, A.; Hebard, A. F. Phys. Rev. Lett. **2009**, 102, 077205.

[17] Kumar, D.; Rajeev, K. P.; Alonso, J. A. Appl. Phys. Lett. **2018**, 112, 133103.

[18] Varignon, J.; Grisolia, M. N.; Íñiguez, J.; Barthélémy, A.; Bibes, M. npj Quantum Materials **2017**, 2, 21.

[19] Mattoni, G.; Zubko, P.; Maccherozzi, F.; Torren, A. J. H. V. D.; Boltje, D. B.; Hadjimichael, M.; Manca, N.; Catalano, S.; Gibert, M.; Liu, Y.; Aarts, J.; Triscone, J.-M.; Dhesi, S. S.; Caviglia, A. D. Nat. Commun. **2016**, 7, 13141.

[20] Preziosi, D.; Lopez-Mir, L.; Li, X.; Cornelissen, T.; Lee, J. H.; Trier, F.; Bouzehouane, K.; Valencia, S.; Gloter, A.; Barthélémy, A.; Bibes, M. Nano Lett. **2018**, 18, 2226−2232.

[21] McLachlan, D. S.; Sauti, G.; J. Nanomat. **2007**, 30389.

[22] Granados, X.; Fontcuberta, J.; Obradors, X.; Manosa, L; Torrance, J. B. Phys. Rev. B **1993**, 48 (16), 666–672.

[23] Catalan, G.; Bowman, R. M.; Gregg, J. M. Phys. Rev. B **2000**, 62, 7892−7900.

[24] Caviglia, A. D.; Forst, M.; Scherwitzl, R.; Khanna, V.; Bromberger, H.; Mankowsky, R.; Singla, R.; Chuang, Y.-D.; Lee, W. S.; Krupin, O.; Schlotter, W. F.; Turner, J. J.; Dakovski, G. L.; Minitti, M. P.; Robinson, J.; Scagnoli, V.; Wilkins, S. B.; Cavill, S. A.; Gibert, M.; Gariglio, S.; Zubko, P.; Triscone, J.-M.; Hill, J. P.; Dhesi, S. S.; Cavalleri, A. Phys. Rev. B **2013**, 88, 220401(R).

[25] Preziosi, D.; Sander, A.; Barthélémy, A.; Bibes, M. AIP Advances **2017**, 7, 015210.

[26] Arora, A.; Phillips, L. C.; Nukala, P.; Hassine, M. B.; Unal, A. A.; Dkhil, B.; Balcells, L.; Iglesias, O.; Barthélémy, A.; Kronast, F.; Bibes, M.; Valencia, S. Phys. Rev. Materials **2019**, 3, 024403.

[27] Kronast, F.; Valencia, S. J. large-scale Res. Facil. **2016**, A90, 1-6;